Reversible Photodoping of TiO$_2$ Nanoparticles for Photochromic Applications

Urmas Joost,[†,‡] Andris Šutka,[‡,§] Marek Oja,[‡] Krisjanis Smits,[∥] Nicola Döbelin,[⊥] Ardi Loot,[‡] Martin Järvekülg,[‡] Mika Hirsimäki,*[,†] Mika Valden,[†] and Ergo Nõmmiste[‡]

[†]Surface Science Group, Laboratory of Photonics, Tampere University, Korkeakoulunkatu 3, FI-33720 Tampere, Finland
[‡]Institute of Physics, University of Tartu, W. Ostwaldi Street 1, EE-50411, Tartu, Estonia
[§]Research Laboratory of Functional Materials Technologies, Faculty of Materials Science and Applied Chemistry, Riga Technical University, Paula Valdena 3/7, Riga LV-1048, Latvia
[∥]Institute of Solid State Physics, University of Latvia, Kengaraga 8, Riga LV-1063, Latvia
[⊥]RMS Foundation, Bischmattstrasse 12, CH-2544 Bettlach, Switzerland

ABSTRACT: Observations on the strong photochromic effect of crystalline TiO$_2$ quantum dots (mean size ≈ 4 nm) are presented. The synthesized quantum dots consist of irregularly shaped anatase TiO$_2$ nanoparticles (NPs) and are dispersed in butanol (8% by mass). Obtained NPs exhibit a dramatic photoresponse to UV light, enabling effective transmittance modulation in a broad wavelength range extending from the visible to near-infrared region, and even the thermal black body radiation regime beyond 10 μm. The exceptional photoresponse is attributed to hole-scavenging by butanol, TiO$_2$ self-reduction, injection of electrons to the conduction band, and consequent localized surface plasmon resonances in NPs. The observed optical effect is reversible, and the initial high transmittance state can be restored simply by exposing the NPs to air. The applied NP synthesis route is economic and can be easily scaled for applications such as smart window technologies.
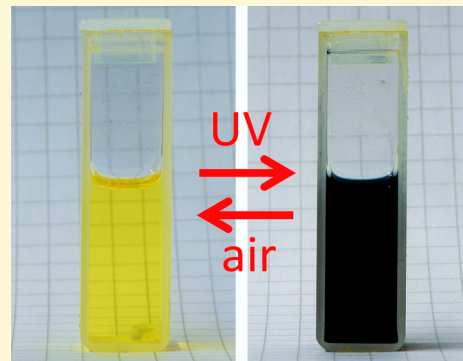
1. INTRODUCTION

Energy management and efficiency are among the key elements of modern building technologies and impact other fields that prioritize optimized consumption such as automotive industry and transportation. Development of highly insulating and adaptive smart windows for applications in both the commercial and residential sector could save about 4.5% of the annual energy consumption.[1] Control over the transmittance of window materials in the visible (VIS) and near-infrared (NIR) part of the spectrum (and even the thermal black body radiation at 10 μm) will have a positive impact on the living comfort (e.g., less glare and thermal discomfort) and energy efficiency in commercial and residential environments as well as in automotive applications.

Various transition metal oxides, such as MoO$_3$, WO$_3$, TiO$_2$, V$_2$O$_5$, NiO/Ni$_2$O$_3$, Nb$_2$O$_5$, etc., exhibit a photoresponse to either sunlight or UV radiation; i.e., a change in transmittance/absorbance manifests itself in apparent color change. Many of the existing photochromic applications are based on tungsten oxide (WO$_3$) or nickel oxides.[2] However, W is a dense material which adds to the weight and indirect costs of the final product. It is also a scarce material, and for instance, the European Union considers W a critical metal with a high supply risk.[3] The low abundancy of W and its potentially adverse impact on the environment and human health drive research for other photochromic materials. While more abundant than W, Ni is also associated with environmental and health risks. Therefore, Ti is attracting increased attention as an abundant, lightweight, nontoxic, and environmentally benign alternative.

The general consensus is that pristine (undoped) TiO$_2$ exhibits little photochromicity. However, it has been shown that TiO$_2$ can be used to enhance the photochromic response of, for instance, WO$_3$ in which it acts as a hole scavenger and electron donor.[4,5] Similarly, V^{5+} doped anatase TiO$_2$ exhibits a photochromic effect. In this case, photogenerated electrons reduce V^{5+} to V^{4+}, leading to a decrease in light transmission that is visible as a color change from beige yellow to brownish-violet.[6] In a photochromic system consisting of Ag nanoparticles on thin TiO$_2$ film, the light absorption can be controlled by oxidizing and photocatalytically reducing the plasmonic Ag particles.[7] A solid-state photochromic device has also been demonstrated where TiO$_2$ acts as a mediator in vectorial electron transfer between the molecular sensitizer and electron acceptor.[8] Finally, it has been shown that nanoscale TiO$_2$ particles and TiO$_2$ gels exhibit partial photoresponse to
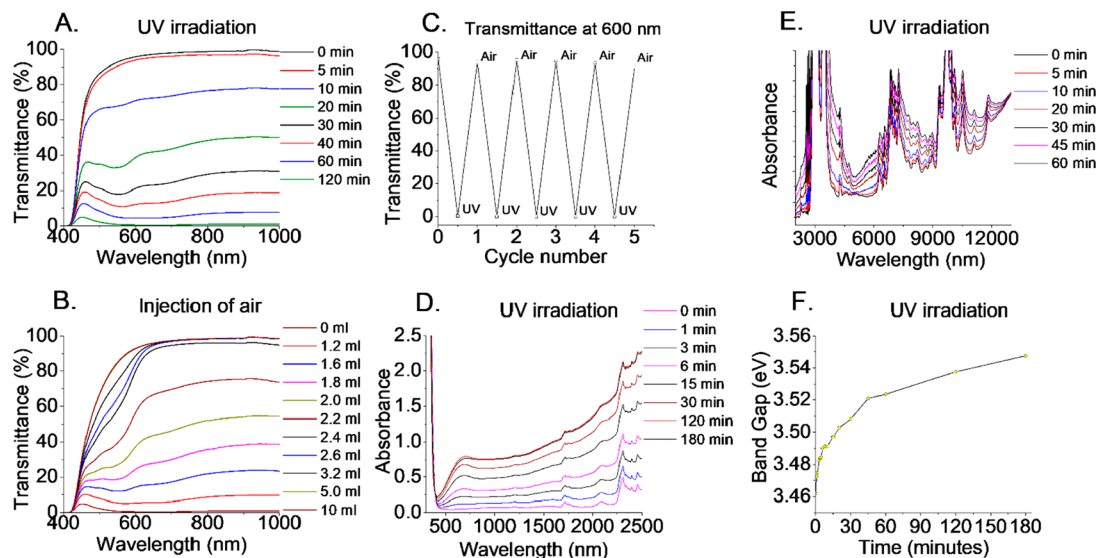
Figure 1. Optical response of TiO$_2$ NPs to (A) UV irradiation and (B) air oxidation. It can be observed that light is more and more obscured, if the TiO$_2$ dispersion is irradiated with UV light. However, the transmittance of the colloid is recovered, if the dispersion is exposed to air. (C) Cycling behavior of the TiO$_2$ NPs dispersion with UV light (2 h per cycle) and air injection (20 mL per cycle). (D) Change in the absorbance of 200 μm layer of TiO$_2$ NP colloid. (E) FT-IR measurements of the NP colloid during UV irradiation. It can be observed that, during UV irradiation, the absorbance values increase up to 12 000 nm. (F) Change in the indirect optical band-gap value of the TiO$_2$ NPs as a function of UV irradiation time.

UV irradiation; i.e., altered transmittance in the visible and near-infrared range is observed due to limited and nonuniform modulation in absorption.[9,10] To the best of our knowledge, the photoresponse achieved in TiO$_2$-based materials does not cover the relevant wavelength range to the extent that is required in applications.

In order to improve on the existing Ti-based photochromic materials, it is imperative to understand the underlying physical phenomena. It is now well understood that photochromicity in transition metal oxides is governed by the redox process arising due to optically excited electron−hole pairs.[6,11,12] In the VIS regime, the light absorption can be attributed to the localization of injected electrons at Ti^{3+} cations which creates polaronic lattice distortions. However, if the density of free charge carriers is sufficiently high, another absorption mechanism activates on nanoscale particles. That is, the onset plasmonic resonance leading to absorption in the infrared (IR) spectral region.[13]

In this study, we report the fabrication of a versatile and affordable photochromic nanomaterial through a readily scalable process. Photochromicity is achieved via structural and electronic phenomena in pristine TiO$_2$ nanoparticles (TiO$_2$ NPs) that—unlike bulk TiO$_2$—make excellent photochromic coatings. In particular, we demonstrate that TiO$_2$ NPs in butanol exhibit a photochromic response that is superior to that of the alternative materials.[4−8] Namely, the transmittance of produced TiO$_2$ NPs varies from 100% to 0% over a broad wavelength range that extends to the thermal black body radiation regime at 10 μm. The simplicity of the active material, the optical properties of the nanoparticles, and the affordability and scalability of the presented synthesis technique make our approach well suited for superior solutions for light transmittance control in building, automotive, and eyewear applications.

2. RESULTS AND DISCUSSION

A photochromic material is expected to exhibit changes in its optical properties in reaction to light. Studied NP dispersions were initially highly transparent and appeared clear to the eye. Measured transmittance was around 95% at 600 nm. Transmittance decreased dramatically during UV exposure. As evident in Figure 1A, the spectral response is smooth without distinct local features, showing almost continuous absorption from the wavelength ranges of visible and near-infrared to mid- and long-infrared. The uniformity of absorption is important as any peaks and valleys in the absorption spectrum ultimately affect not only the efficiency but also the visual appearance of the material that is critical in applications. In our case, TiO$_2$ NPs were rendered visually black upon exposure to UV light.

In general, we attribute the observed optical effect to a photochemical reaction where the UV radiation excited electron−hole pairs and the holes are subsequently scavenged by butanol.[14] Photoexcited electrons populate the conduction band, as well as reduce some Ti^{4+} to Ti^{3+} in the anatase lattice. The entire photochemical reaction mechanism can be expressed by

$$TiO_2 + h\nu \rightarrow e^-_{CB} + h^+_{VB} \tag{1}$$

$$e^-_{CB} + Ti^{4+} \rightarrow Ti^{3+} \tag{2}$$

$$h^+_{VB} + OHCH_2R \rightarrow H^+ + R\overset{\bullet}{C}HOH \tag{3}$$

Free electrons are responsible for absorption in the IR spectral region due to plasmonic resonance,[13] and different Ti^{3+} species form defect states at different energies in the band gap of anatase.[15] Formation of Ti^{3+} is compensated by oxygen vacancies in accordance with the equation

$$Ti_2O_3 \xrightarrow{TiO_2} 2Ti(III)'_{Ti(IV)} + 3O^x_O + V^{\bullet\bullet}_O \tag{4}$$
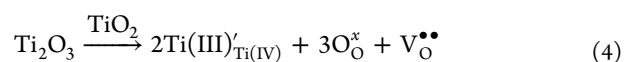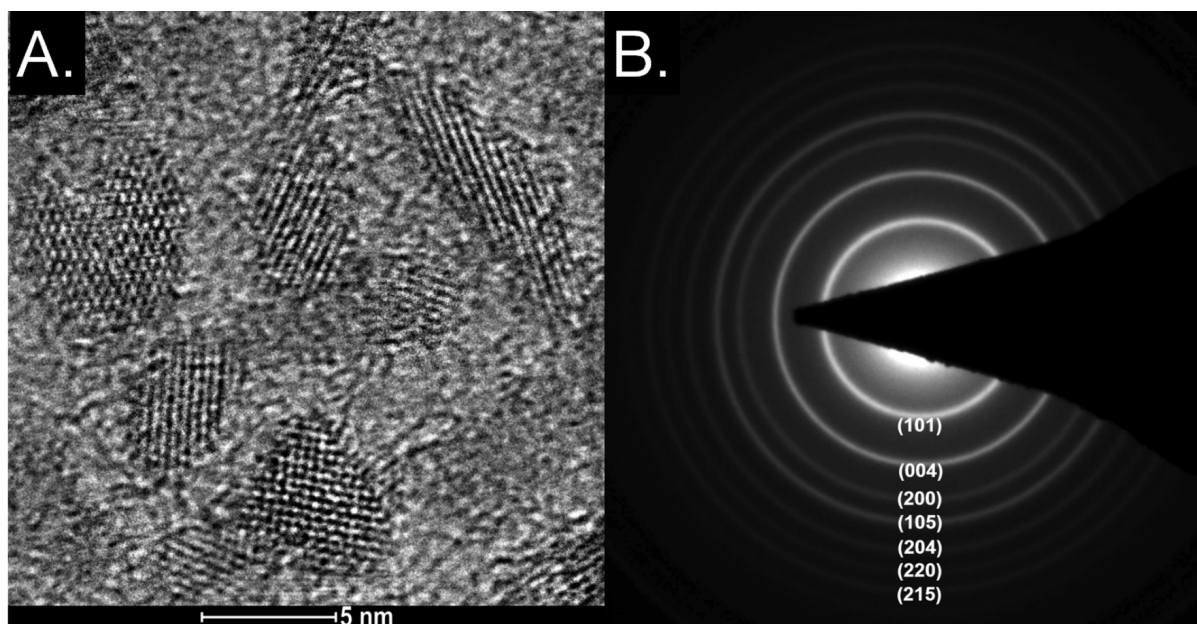
Figure 2. (A) TEM image of the TiO$_2$ NPs shows the presence of elongated crystalline particles. (B) Electron diffraction pattern obtained from the TiO$_2$ NP-s. The diffraction pattern indicates that the anatase particles are crystalline.[19]

Oxygen vacancy species also form intragap states and are responsible for visible light absorption of black TiO$_2$.[16] Recently, visible light absorption was observed in hydrogenated TiO$_2$ that was attributed to the formation of a disordered layer on the surface of nanoparticles, causing valence band tailing.[17] It is suggested that electronic transitions from localized states of both the tailed valence band and oxygen vacancies to the conduction band, and from the tailed valence band to oxygen vacancies, are responsible for the visible light absorption in TiO$_2$.[16] Our system includes a protic solvent which could lead to TiO$_2$ hydrogenation during UV irradiation.

The rate at which the optical properties change upon external stimulus and the reversibility of induced effects are among the key factors in the functionality of photochromic materials. As evident in Figure 1A, our NPs exhibit a fairly fast response to UV irradiation. It takes approximately 15 min to reach optical transmittance of 52%. After 120 min of UV irradiation, the transmittance at 600 nm is less than 0.5%. The delay in the spectral change in the first 5 min of UV irradiation can be explained by the presence of adsorbed oxygen species on the NPs surface. Electron paramagnetic resonance (EPR) results exhibited a signal related to Ti^{4+}-O^{2-} centers before UV irradiation. The signal disappeared during UV irradiation. Optical transmittance curves are relatively flat and featureless. The visual appearance of the dispersions is black with a slight bluish tint.

Figure 1B also suggests that the photochromic effect is fully reversible. The initial high transmissivity can be restored by injecting air into the dispersion as shown in Figure 1C. Hence, the dispersion can be successfully cycled between transmitting and absorbing states, indicating that the material is suitable for applications where fast switching is not as critical as uniform spectral response and affordability of the material. It is also worth pointing out that the suspensions were stable and did not sediment during long-term cycling.

Interestingly, the speed of recovery varies along the entire absorption spectrum (Figure 1B). The transmittance in the IR part of the spectrum recovers significantly faster than in the visible part of the spectrum. This important observation suggests that at least two different mechanisms determine the transmissivity of the TiO$_2$ NP colloid. As discussed earlier, it is reasonable to attribute light absorption in the VIS regime to polaronic lattice distortions in TiO$_2$. Surface plasmons, on the other hand, are known to readily absorb light in IR range as well as exhibit high sensitivity to adsorbing molecules.[18] In contrast to surface plasmons, the electrons trapped at polaronic lattice distortions are likely to be far less sensitive to adsorbed species. However, the onset of surface plasmon resonances requires a sufficiently high density of free charge carriers,[13] and this requirement is not satisfied on TiO$_2$ NPs intrinsically. Before addressing this question, we shall first explore the optical response of NPs in more detail.

To study the response of the NPs in a wider spectral region and using higher UV dosages, a sealed cuvette with a 200 μm PTFE separator was used to measure the response of the NPs up to 2500 nm wavelengths. Thin samples were prepared from the dispersions to counteract the absorption maxima of the solvent in the NIR range and to make it possible to irradiate the material with higher doses of UV per volume. The cuvettes were filled with the TiO$_2$ dispersion in a nitrogen atmosphere in a glovebox (O$_2$ concentration > 0.5 ppm) and sealed with epoxy resin. The cuvette was irradiated with the same UV diode as in previous experiments with the power density of UV-A radiation set to 30 W/m^2 which coincides with the UV-A intensity of sunlight on Earth.

As can be seen in Figure 1D, the absorbance increases during UV irradiation. The spectra are smooth and have no distinct extrema besides the absorbance bands of the solvent butanol in the NIR region. The increase in absorbance during UV irradiation is more prominent in the NIR region than in the visible range. The optical response in a thin dispersion layer was reasonably rapid; absorbance at 600 nm increased from 0.05 to 0.46 in 15 min. The absorbance of the layers becomes saturated after 3 h of irradiation at 0.65 absorbance units.

To further characterize the optical properties of NPs in the IR range, an ATR FT-IR spectrometer was used to measure the spectral response. A drop of the dispersion was first placed on the ATR crystal. A PTFE ring was then placed around the crystal to act as a support for a 1 mm thick soda-lime glass cover. The dispersion was irradiated through the glass with the UV diode. Due to the nature of the ATR setup, it was impossible to quantitatively compare the FT-IR spectra to the UV−VIS−NIR spectra. However, the FT-IR spectra still yield valuable information about the trends and behavior of the NPs in the IR region. The results of the more detailed study of IR absorption during UV irradiation (Figure 1E) show that the increase in absorption extends to 12 000 nm.

The transmittance of TiO_2 NP dispersions can thus be modulated by photodoping and air oxidation to transmit or block VIS light, solar NIR light, and even the black body radiation from objects at room temperature. A smooth and steadily increasing background is also present. It stems from the increase in absorbance of the NPs as a function of UV exposure. The strong IR absorbance bands observed in Figure 1E are attributed to the solvent butanol.

To gain deeper insights into the physical origins of the observed absorption phenomena, we conducted a more detailed analysis of UV−VIS spectra. We found that UV irradiation influences the indirect band gap[20] of the anatase TiO_2 NPs. In particular, when Tauc plots were used to determine the optical band gaps of dispersions, we observed (Figure 1F) that the indirect band gap increases during UV exposure. This effect can be explained by the Burstein−Moss shift:[21] as the electronic states near the conduction band bottom become increasingly populated, both the absorption edge and the apparent band gap are increased.

The structure and structural stability of the particles are important for the applicability of a photochromic material. The transmission electron microscope (TEM) image in Figure 2A shows oblong crystalline TiO_2 NPs of 5−10 nm length and 2−5 nm width. The results coincide well with dynamic light scattering (DLS, Figure S1) and X-ray diffraction (XRD, Figure S2) results. DLS measurements show that the average diameter of the particles by volume is 4.3 nm and it remains constant when the material is cycled. In the TEM images, we also observe lattice fringes, suggesting that the material is crystalline. X-ray diffraction patterns show very broad peaks (Figure S2). The low intensity of the maxima can be attributed to the small particle size and low concentration of particles in the suspension (8% by mass). The severe peak broadening is a result of the nanometer-range size of crystallites and particles. Nevertheless, the phase is clearly identifiable as anatase (TiO_2, PDF # 04-007-0701, ICDD database), and Rietveld refinement allowed us to determine the unit cell dimensions and average crystallite sizes (Table 1). The results indicate no significant variation in lattice structure when the material is cycled between the transparent and absorbing states under UV radiation, ruling out the occurrence of photocorrosion. The samples were stable during measurements, and we observed no X-ray (λ = 1.54056 Å) induced changes in the transmittance of the sample. The crystalline nature of the particles is also confirmed by fringes in the electron diffraction pattern (Figure 2B). Rietveld analysis (Table 1) also suggests that the particles are stable and UV irradiation causes no changes in the lattice parameters.

With the optical and structural properties of the NPs now addressed, we can return to their electronic properties.

Table 1. Refined Crystallographic Parameters of the Clear and UV-Irradiated Black Suspension As Obtained by X-ray Diffraction[a]

	clear suspension	black suspension
phase composition	100% TiO_2 anatase	100% TiO_2 anatase
unit cell dimensions [Å]	a = 3.7978 (0.0019)	a = 3.7959 (0.0019)
	c = 9.4905 (0.0055)	c = 9.4929 (0.0051)
average crystallite size [nm]	5.1(0.1)	5.0(0.1)

[a]Estimated standard deviations as reported by the Rietveld refinement software are given in parentheses.

2.1. Absorption in VIS Regime. As we proposed earlier, light absorption in the visible region by TiO_2 is likely due to the localization of injected electrons at Ti^{3+} cations, which creates polaronic lattice distortions by elongating Ti−O bonds. This structural distortion is necessary to achieve localization at a single ion, and clearly demonstrates the polaronic nature of the Ti^{3+} species.[15]

In Figure 3A, we present EPR spectra before and after irradiation with UV. Before irradiation, absorption at g values 2.026, 2.0096, and 2.0036 was observed. These values correspond to Ti^{4+}-O^{2-} species in anatase.[22] During UV irradiation, the signal corresponding to Ti^{4+}-O^{2-} species disappears and is replaced by a strong signal with g = 1.957 which corresponds to Ti^{3+} species,[23] which suggests that exposure to light does, indeed, create polaronic lattice distortions on NPs. The low intensity bands at both sides of the main signal correspond to overlapping Ti47 (I = 5/2) and Ti49 (I = 7/2) hyperfine splitting with a hyperfine coupling constant of 47 MHz. It is important to note that no Ti^{3+} is visible in the EPR spectrum before UV irradiation. This result was also confirmed by X-ray photoelectron spectroscopy (XPS, Figure S3) where Ti core levels showed no evidence of Ti^{3+} prior to UV irradiation.

The number of photoelectrons was obtained via Redox titration with Fe^{3+} complexes (Figure S4). The same method has been previously used by Schimpf et al.[24] to successfully determine the amount of photogenerated electrons in ZnO nanoparticles. In our case, a diluted sample (0.5% mass % of TiO_2) of the dispersion was irradiated with UV radiation to a point where the absorbance value of the dispersion did not increase, and then titrated with Fe(acac)$_3$. The end point of the titration was determined using a photospectrometer (Cary 5000) by recording sequential absorbance spectra of the dispersion as the Fe^{3+} complex was added.

In our study, the redox titration (Figure S4) yields a number of 0.015 electrons generated per every titanium atom. This gives us an electron density of 5×10^{20} cm^{-3}. The number of electrons trapped at Ti^{3+} sites can be estimated from the EPR spectra. We find this to be as low as 2.5×10^{18} cm^{-3}. Hence, only a small portion (approximately 0.5%) of available charge carriers are, in fact, trapped as Ti^{3+}, leaving the majority of electrons as free charge carriers.

The strong visible light absorption of UV irradiated nanocrystals let us to assume that there are additional absorption levels in the TiO_2 band gap originating from lattice defects. Electronegativity can be preserved due to oxygen vacancies compensating Ti^{3+}, as well as hydrogenation due to protic medium.

2.2. Absorption in IR Regime. The earlier observation that the IR part of the absorption spectrum is highly sensitive to air (Figure 1B) is instrumental in understanding the
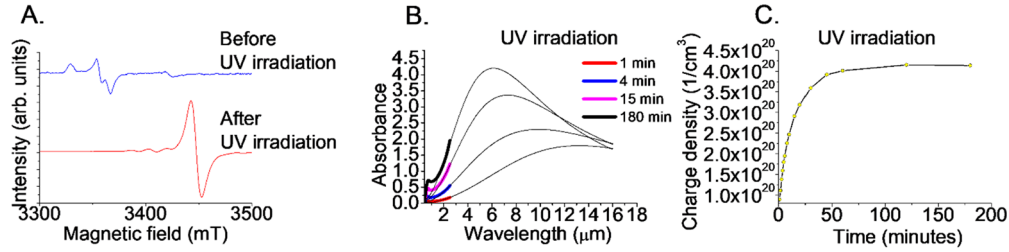
Figure 3. (A) EPR spectra before UV irradiation (blue) and after UV irradiation (red). (B) Comparison of experimental absorbance values with absorbance calculated using Mie theory. (C) The subsequent charge densities extracted from the data.

provided clues to the respective roles of the free and localized charge carriers in light absorption processes. Absorption in the visible part of the spectrum was found to be less reactive toward air exposure, but there was a strong concomitant decrease in absorption in the IR part of the spectrum. We argue that both observations can be attributed to the reactivity of trapped and free electrons toward oxygen in the air. The trapped electrons are already bound to Ti^{3+} and are therefore less reactive. As a result, absorption in the VIS range shows less sensitivity to air. In contrast, the above-mentioned delocalized (free) electrons are likely to be highly reactive toward oxygen. Exposure to air led to a rapid decrease in IR absorbance, suggesting that these free electrons play an important role in the absorption in that particular spectral region. Similar optical effects—reversible switching of plasmonic absorption by light irradiation and redox reactions—have also been observed in ZnO nanoparticles.[25]

Localized surface plasmon resonance (LSPR) provides a plausible explanation for the observed absorption in the IR region and the influence of air exposure. In general, LSRP is a collective electronic excitation induced by electromagnetic radiation on metallic nanoparticles, but it can also occur on oxide nanoparticles if there is a significant local density of free charge carriers. In our case, the presence of excess electrons has been demonstrated with redox titration, and it is conceivable that their interaction with light results in LSPRs that play a role in the absorbance of IR light.

To confirm and quantify the contribution of LSPR to the absorption, an analogous methodology was used as utilized by Luther et al.[26] Mie scattering theory can be employed to calculate the absorption cross section σ of a single particle, and Beer−Lambert law allows us to calculate the absorbance of the suspension caused by LSPR

$$A_{sp} = N\sigma l \tag{5}$$

where N is the concentration of spheres and l is the path length of the beam in the sample.

In order to use Mie scattering theory, the electrical permittivity ε of the particles must be estimated. As a standard solution, we use the Drude model, which relates the concentration of free electrons N_e, losses γ, and high frequency permittivity ε_∞ through the equation

$$\varepsilon(\omega) = \varepsilon - \frac{\omega_p^2}{\omega^2 + i\gamma\omega} \tag{6}$$

where $\omega_p = \sqrt{N_e e^2/(\varepsilon_0 m_e)}$ is plasma frequency, e and m_e are the charge and mass of the free electrons, respectively, and ε_0 is the free space permittivity. In this study, we fix $\varepsilon_0 = 10$ and let

the concentration of free charges N_e and the loss factor γ to be free fitting parameters.

There are some limitations to the Mie scattering theory. For instance, it only allows us to calculate the absorption/scattering cross section for a spherical particle, while our TiO_2 NPs are neither spherical nor uniform in size. However, it is evident via direct Mie calculations that, in the case of very small particles (in our case, <10 nm; see Figure 2A), the width of the modeled LSPR does not depend on the particle size. Here, we used an average diameter of 4 nm and took into account that the concentration of the spheres N in the Beer−Lambert law is only an effective value and does not influence the shape of the absorbance spectrum.

To compare the results from our model to the experimental results, we must first extract the absorbance caused by the plasmonic resonances. As the absorption cross section of dielectric spheres is small in comparison to the plasmonic particles, the absorbance caused by LSPR is extracted by subtracting the absorbance at the time $t = 0$ min (see Figure 3B). As a simplification, it is assumed that the LSPR is the only source of the increase in the absorbance in the IR range.

The experimentally measured absorbance caused by the UV radiation over time is shown in Figure 3B in colored lines. By fitting the model to the experimental data, it is possible to explain the absorbance in the NIR part (solid bold lines). The model breaks down in the visible spectral region, where absorption is linked to the localization of injected electrons on Ti^{3+} cations that creates polaronic lattice distortion. The dependence of the free charge density N_e on the irradiation time is extracted from the model and shown in Figure 3C. The estimated number of free electrons is well within the range required for surface plasmonic resonances to occur and therefore strongly supports our earlier hypothesis of surface plasmons being responsible for IR absorption. As can be seen in Figure 3C, the maximum free charge carrier density extracted from the theoretical model coincides well with the value found experimentally by redox titration (5×10^{20} cm^{-3}).

3. CONCLUSIONS

In this work, we have demonstrated a cost-effective way of preparing TiO_2 NP dispersions that have superior photochromic functionality. We have demonstrated that the transmittance of the NPs can be strongly modulated in a wide optical range from 400 to 12 000 nm (i.e., from visible spectrum to MIR) and identified two distinct physical mechanisms that explain the observed phenomena. We found that the exposure to light generates polaronic lattice distortions in NPs and they determine the transmittance in the visible region of the spectrum. The second absorption mechanism originates from the photoreduction of TiO_2 during UV irradiation and causes photochromism in the IR part of the

spectrum. The photoreduction of TiO_2 leads to the formation of Ti^{3+}, but only a small fraction of the photogenerated electrons is trapped as Ti^{3+} (approximately 0.5%). The majority of photogenerated electrons remains free charge carriers. The availability of free charge carriers in the proximity of TiO_2 NPs under UV irradiation results in the onset of localized surface plasmon resonances, which readily absorb light in the IR regime.

The observed even absorption of our photoreduced TiO_2 NPs in a wide range makes them eminently suitable for photochromic applications, where modulation of the material's transmittance uniformly over the entire VIS and IR region and cycling between transmitting and absorbing states are desired. Our findings open up new avenues for energy efficiency and lighting/thermal control in building and automotive applications.

4. METHODS

4.1. Synthesis of Titania Nanoparticles. NPs were synthesized using a method described by Scolan and Sanchez[27] with slightly modified parameters. Commercially available reagents titanium(IV) butoxide (Sigma-Aldrich, reagent grade), dodecyl benzene sulfonic acid (DBSA) (Sigma-Aldrich, reagent plus), acetyl acetone (acac) (Sigma-Aldrich, reagent plus), butanol (Sigma-Aldrich), and deionized water were used as precursors. The solvent (butanol) was dried using CaH_2 and distilled before use. The molar ratio between DBSA and titanium(IV) butoxide was set to 0.2, that between acac and titanium(IV) butoxide was set to 3, and that between water and titanium(IV) butoxide was set to 10. The reaction was carried out overnight at reflux conditions. The nanoparticles were purified twice with methanol using centrifugation at $2000g$ for 1 h. The synthesis was optimized to obtain highly crystalline nanoparticles (roughly 3–10 nm in diameter). NP yield of developed synthesis protocol exceeded 85% after washing procedures.

4.2. Optical Characterization. Optical transmission measurements were conducted on a Cary 5000 (UV/VIS/NIR) spectrometer (Agilent Technologies). Experiments were conducted in a 10 mm optical path length quartz cuvette; 2 mL of 8% (by mass) TiO_2 NP suspension was placed inside the spectrometer measurement chamber. The cuvette was equipped with a magnetic stir bar and UV diode (P8D136, Seoul Semiconductors, 365 nm). The UV diode was operated at 300 mA. The cuvette was sealed by an airtight cap. For subsequent air injection, a small tube ($d \sim 0.8$ mm) leading to the bottom was inserted at the corner of the cuvette. Air was pumped into the cuvette using a syringe pump at 1 mL/min. The dispersions were purged with 20 mL of nitrogen before the start of experiment to remove residual oxygen from the cuvette.

Measurements were also conducted on thin NP dispersion layers. The samples were irradiated using the UV diode with 30 W/m^2 light intensity. The cell consisted of two glass plates separated by a 200 μm PTFE separator. The cell volume was minimized to allow for larger irradiation dosages and to minimize the interference from the NIR absorbance bands of the solvent. Also, the dispersion concentration was increased to 20% by mass.

The FT-IR measurements were conducted on a Bruker Vertex V 70 equipped with an ATR accessory. The NP dispersion (sample) was placed onto the ATR crystal (diamond crystal), a 200 μm PTFE separator was placed around the crystal, and a glass plate was pushed onto the NP dispersion so that an airtight compartment was formed on the ATR crystal. The sample was irradiated through the glass plate using the same UV diode that was utilized in the UV−VIS measurements.

4.3. Electron Paramagnetic Resonance (EPR). Electron paramagnetic resonance measurements were performed using a Bruker X-band E500 CW (con-tinuous wave) ELEXSYS spectrometer at room temperature (297 K). The microwave frequency during the measurements was 9.8 GHz. The Bruker quantative EPR toolbox in the Bruker Xepr program was used for quantitative analysis. The TiO_2 NP suspension was injected to a quartz tube suitable for liquid EPR measurements. The sample was irradiated using the same UV diode that was also in use in the UV−VIS mesurements.

4.4. X-ray Diffraction (XRD). The crystalline phase of the synthesized particles prior and after UV irradiation was determined by XRD on a Bruker D8 diffractometer (Bruker, Karlsruhe, Germany) CuKα radiation. The suspension was injected into a glass capillary (480 μm inner diameter, Hilgenberg special glass No. 10, Hilgenberg, Germany), which was then sealed by dipping both ends in molten paraffin. Data were measured from $20-100°$ 2θ with a step size of $0.0122°$ 2θ and a counting time of 8 s per step, resulting in total acquisition time of nearly 15 h. A second capillary was filled and sealed, and subsequently exposed to UV radiation (254 nm, 5×8 W) for 10 h prior to XRD data collection. The data sets were evaluated by Rietveld refinement using the software Profex (version 3.8)[28] with the Rietveld kernel BGMN (version 4.2.22).[29]

4.5. X-ray Photoelectron Spectroscopy (XPS). XPS was used for investigating the chemical state and elemental composition of titania NP films. The films were prepared from the same dispersions by spin-coating them on Si(100) monocrystal substrates. XPS measurements were conducted using a surface station equipped with an electron energy analyzer (SCIENTA SES 100) and a nonmonochromatic twin anode X-ray tube (Thermo XR3E2), with a characteristic energy of 1253.6 eV (Mg K$\alpha_{1,2}$, fwhm 0.68 eV). All XPS measurements were conducted in Ultra-High Vacuum (UHV) with a base pressure better than 8×10^{-10} mbar.

■ REFERENCES

(1) Gillaspie, D. T.; Tenent, R. C.; Dillon, A. C. Metal-oxide Films for Electrochromic Applications: Present Technology and Future Directions. *J. Mater. Chem.* **2010**, *20*, 9585−9592.

(2) Niklasson, G. A.; Granqvist, C. G. Electrochromics for Smart Windows: Thin Films of Tungsten Oxide and Nickel Oxide, and Devices Based on These. *J. Mater. Chem.* **2007**, *17*, 127−156.

(3) *COMMUNICATION FROM THE COMMISSION TO THE EUROPEAN PARLIAMENT, THE COUNCIL, THE EUROPEAN ECONOMIC AND SOCIAL COMMITTEE AND THE COMMITTEE OF THE REGIONS on the 2017 list of Critical Raw Materials for the EU*; Document 52017DC0490; European Commission: Brussels, Belgium, 2017. https://eur-lex.europa.eu/legal-content/EN/TXT/?uri=CELEX:52017DC0490 (accessed on Nov 28, 2018).

(4) He, Y.; Wu, Z.; Fu, L.; Li, C.; Miao, Y.; Cao, L.; Fan, H.; Zou, B. Photochromism and Size Effect of WO_3 and WO_3−TiO_2 Aqueous. *Chem. Mater.* **2003**, *15*, 4039−4045.

(5) He, T.; Ma, Y.; Cao, Y.; Hu, X.; Liu, H.; Zhang, G.; Yang, W.; Yao, J. Photochromism of WO_3 Colloids Combined with TiO_2 Nanoparticles. *J. Phys. Chem. B* **2002**, *106*, 12670−12676.

(6) Songara, S.; Patra, M. K.; Manoth, M.; Saini, L.; Gupta, V.; Gowd, G. S.; Vadera, S. R.; Kumar, N. Synthesis and Studies on Photochromic Properties of Vanadium Doped TiO_2 Nanoparticles. *J. Photochem. Photobiol., A* **2010**, *209*, 68−73.

(7) Ohko, Y.; Tatsuma, T.; Fujii, T.; Naoi, K.; Niwa, C.; Kubota, Y.; Fujishima, A. Multicolour Photochromism of TiO_2 Films Loaded with Silver Nanoparticles. *Nat. Mater.* **2003**, *2*, 29−31.

(8) Biancardo, M.; Argazzi, R.; Bignozzi, C. A. Solid-State Photochromic Device Based on Nanocrystalline TiO_2 Functionalized with Electron Donor−Acceptor Species. *Inorg. Chem.* **2005**, *44*, 9619−9621.

(9) Kormann, C.; Bahnemann, D. W.; Hoffmann, M. R. Preparation and Characterization of Quantum-Size Titanium Dioxide. *J. Phys. Chem.* **1988**, *92*, 5196−5201.

(10) Castellano, F. N.; Stipkala, J. M.; Friedman, L. A.; Meyer, G. J. Spectroscopic and Excited-State Properties of Titanium Dioxide gels. *Chem. Mater.* **1994**, *6*, 2123−2129.

(11) He, T.; Yao, J. N. Photochromism in Transition-Metal Oxides. *Res. Chem. Intermed.* **2004**, *30*, 459−488.

(12) Dahlman, C. J.; Tan, Y.; Marcus, M. A.; Milliron, D. J. Spectroelectrochemical Signatures of Capacitive Charging and Ion Insertion in Doped Anatase Titania Nanocrystals. *J. Am. Chem. Soc.* **2015**, *137*, 9160−9166.

(13) De Trizio, L.; Buonsanti, R.; Schimpf, A. M.; Llordes, A.; Gamelin, D. R.; Simonutti, R.; Milliron, D. J. Nb-Doped Colloidal TiO_2 Nanocrystals with Tunable Infrared Absorption. *Chem. Mater.* **2013**, *25*, 3383−3390.

(14) Di Valentin, C.; Fittipaldi, D. Hole Scavenging by Organic Adsorbates on the TiO2 Surface: A DFT Model Study. *J. Phys. Chem. Lett.* **2013**, *4*, 1901−1906.

(15) Di Valentin, C.; Pacchioni, G.; Selloni, A. Reduced and n-Type Doped TiO2: Nature of Ti^{3+} Species. *J. Phys. Chem. C* **2009**, *113*, 20543−20552.

(16) Naldoni, A.; Allieta, M.; Santangelo, S.; Marelli, M.; Fabbri, F.; Cappelli, S.; Bianchi, C. L.; Psaro, R.; Dal Santo, V. Effect of Nature and Location of Defects on Bandgap Narrowing in Black TiO_2 Nanoparticles. *J. Am. Chem. Soc.* **2012**, *134*, 7600−7603.

(17) Chen, X.; Liu, L.; Yu, P. Y.; Mao, S. S. Increasing Solar Absorption for Photocatalysis with Black Hydrogenated Titanium Dioxide Nanocrystals. *Science* **2011**, *331*, 746−750.

(18) Mayer, K. M.; Hafner, J. H. Localized Surface Plasmon Resonance Sensors. *Chem. Rev.* **2011**, *111*, 3828−3857.

(19) Sedach, P. A.; Gordon, T. J.; Sayed, S. Y.; Fürstenhaupt, T.; Sui, R.; Baumgartner, T.; Berlinguette, C. P. Solution Growth of Anatase TiO_2 Nanowires from Transparent Conducting Glass Substrates. *J. Mater. Chem.* **2010**, *20*, 5063−5069.

(20) Reyes-Coronado, D.; Rodríguez-Gattorno, G.; Espinosa-Pesqueira, M. E.; Cab, C.; de Coss, R.; Oskam, G. Phase-pure TiO_2 Nanoparticles: Anatase, Brookite and Rutile. *Nanotechnology* **2008**, *19*, 145605.

(21) Saw, K. G.; Aznan, N. M.; Yam, F. K.; Ng, S. S.; Pung, S. Y. New Insights on the Burstein-Moss Shift and Band Gap Narrowing in Indium-Doped Zinc Oxide Thin Films. *PLoS One* **2015**, *10*, No. e0141180.

(22) Coronado, J. M.; Maira, A. J.; Conesa, J. C.; Yeung, K. L.; Augugliaro, V.; Soria, J. EPR Study of the Surface Characteristics of Nanostructured TiO_2 under UV Irradiation. *Langmuir* **2001**, *17*, 5368.

(23) Yan, Y.; Han, M.; Konkin, A.; Koppe, T.; Wang, D.; Andreu, T.; Chen, G.; Vetter, U.; Morante, J. R.; Schaaf, P. Slightly Hydrogenated TiO_2 with Enhanced Photocatalytic Performance. *J. Mater. Chem. A* **2014**, *2*, 12708−12716.

(24) Schimpf, A. M.; Gunthardt, C. E.; Rinehart, J. D.; Mayer, J. M.; Gamelin, D. R. Controlling Carrier Densities in Photochemically Reduced Colloidal ZnO Nanocrystals: Size Dependence and Role of the Hole Quencher. *J. Am. Chem. Soc.* **2013**, *135*, 16569−16577.

(25) Faucheaux, J. A.; Jain, P. K. Plasmons in Photocharged ZnO Nanocrystals Revealing the Nature of Charge Dynamics. *J. Phys. Chem. Lett.* **2013**, *4*, 3024−3030.

(26) Luther, J. M.; Jain, P. K.; Ewers, T.; Alivisatos, A. P. Localized Surface Plasmon Resonances Arising from Free Carriers in Doped Quantum Dots. *Nat. Mater.* **2011**, *10*, 361−366.

(27) Scolan, E.; Sanchez, C. Synthesis and Characterization of Surface-Protected Nanocrystalline Titania Particles. *Chem. Mater.* **1998**, *10*, 3217−3223.

(28) Doebelin, N.; Kleeberg, R. Profex: a Graphical User Interface for the Rietveld Refinement Program BGMN. *J. Appl. Crystallogr.* **2015**, *48*, 1573−1580.

(29) Bergmann, J.; Friedel, P.; Kleeberg, R. BGMN - A New Fundamental Parameters Based Rietveld Program for Laboratory X-ray Sources, it's Use in Quantitative Analysis and Structure Investigations. In *Commission on Powder Diffraction (IUCr) Newsletter*; IUCr: Chester, U.K., 1998; No. 20, pp 5−8.